

Engineered Nanoparticles Induce DNA Damage in Primary Human Skin Cells, Even at Low Doses

Amelia A. Romoser*, Michael F. Criscitiello*,[†]
and Christie M. Sayes*,^{‡,§}

**Interdisciplinary Program of Toxicology, Texas A&M University
College Station, TX 77843, USA*

*[†]Comparative Immunogenetics Laboratory
Department of Veterinary Pathobiology
Texas A&M University, College Station, TX 77843, USA*

*[‡]Center for Aerosol & Nanomaterials Engineering
RTI International, RTP, NC 27709, USA*

[§]csayes@rti.org

Received 4 June 2013

Accepted 20 September 2013

Published 2 December 2013

It is well documented that various particulate matter — either incidental or engineered — are known to generate reactive oxygen species (ROS) in living cells. In circumstances where these reactive species are generated, antioxidant production is often increased. This balance in the biological reduction/oxidation (a.k.a. redox) state within the cell has not been thoroughly studied in exposures involving engineered nanoparticles. However, nanoparticle exposure has been postulated to induce a DNA damage cascade. In this study, we examined primary human dermal fibroblasts (HDF) exposed to three different, but commonly used engineered nanoparticles (i.e., cerium dioxide (CeO₂), titanium dioxide (TiO₂) and zinc oxide (ZnO)) in an attempt to determine the potential DNA damaging effects through the analysis of ROS generation, relevant protein upregulation response and single and double DNA strand breaks. Cell death was most elevated with exposure to ZnO, followed by TiO₂ and CeO₂. ROS generation was measured at 1 h, 6 h and 24 h after exposure to particles via a cell-based DCFH-DA (2', 7'-dichlorofluorescein-diacetate) assay and indicated that ZnO generated the most significant amount of ROS. ZnO also caused upregulation of oxidative stress protein, heme oxygenase-1 and phosphorylation of p38; whereas CeO₂ caused upregulation of superoxide dismutase. Results from the comet assay indicated that ZnO triggered significant DNA damage in cells at relatively low dosing concentrations (20 ppm). Immunocytochemistry with ZnO-treated cells revealed notable DNA double strand breaks evidenced by a marked increase in the presence of γ -H2AX foci. This finding was also indicated by western blot, as well as cell cycle arrest by the phosphorylation of cyclin-dependent kinase 1. These data suggest that the three particle-types induce different degrees of DNA damage. And, of the three particle-types tested, exposure to ZnO nanoparticles may cause the most significant DNA damage.

Keywords: Cerium dioxide; titanium dioxide; zinc oxide; nanoparticles; dermal; ROS; DNA damage.

1. Introduction

Engineered nanoparticles are often defined as novel materials that have at least one dimension less than 100 nm and exhibit physical and chemical properties not shared by larger fine-sized particles of the same chemical composition.^{1–4} The actual dimensional threshold whereby these new properties can be seen is still a matter of debate. One study has reported that as metal and metal oxide colloidal particles approach 30 nm in diameter or less, the physical and/or chemical properties change significantly from particles of the same chemical composition but larger diameters.⁵ At this size scale, the much larger particle surface-to-volume ratio plays a significant role in interaction at the biological interface. There is a greater potential for nanoparticles to cross cell walls and penetrate the blood-brain barrier.⁶ Due to the “nonbulk” properties of nanoparticles, including their atypical surface structure and surface reactivity, processes such as dissolution, redox reactions and the generation of reactive oxygen species (ROS) may be enhanced. Such properties may elicit biological responses that would not be produced by larger particles of the same chemical composition. Nanotechnology is among the fastest growing areas of scientific research and has important applications in a wide variety of fields. The nanotechnology industry is expected to generate revenues between \$2.6 trillion and \$3.1 trillion by the years 2014 and 2015, respectively.^{7,8}

Nanoparticles are present in many products that come into contact with human skin. Relevant to this research, TiO₂ and ZnO are present in many sunscreens to protect against UV-induced skin damage. Metal oxides do not undergo any chemical decomposition as organic compounds do when exposed to UV radiation, which makes them an attractive alternative.^{9,10} Additionally, they offer a more complete range of protection compared to other products of organic nature.^{11,12} Recently, more products for dermal application utilize finer, nanosized TiO₂ and ZnO since they are transparent and more esthetically pleasing to consumers at this size. TiO₂ nanoparticles are also used in other products that present dermal contact exposures, such as clothing and surface cleaning agents. CeO₂ nanoparticles have proposed and currently used in the areas of biomedicine, cosmetic products, polishing materials and automotive fuel additives.^{13–16} Opportunities for these types of nanoparticle exposures are increasing on a daily

basis,¹⁷ as the products containing these materials are quite common and society is increasingly aware of the importance of UV protection, in general, and the use of improved materials. Since little is known regarding the mechanisms of toxicity for these materials, more research is necessary. The data that has been presented up to now in the literature are sparse and contradictory regarding the effects of nanoparticle exposure in dermal models.

A growing number of studies have investigated the ability of nanoparticles to penetrate skin.^{18–32} The skin is often considered less permeable and the risk perception by this route is generally less than that of respiratory exposure.^{27,33–36} However, in the literature there are studies which suggest that the skin is an important route for the entry of nanoparticles both in occupational and consumer settings^{19,28,37–39} and it has been specifically shown that certain particles are more prone to dermal penetration based upon their physicochemical properties or the nature of the vehicle they are suspended.^{23,32} Bennat and Müller-Goymann found that different formulations had different penetration abilities: according to their experiments, microfine TiO₂ penetrated deeper into human skin from an oily dispersion than from an aqueous one, and encapsulation of the pigments into liposomes caused a higher penetration into the skin.⁴⁰ Furthermore, penetration was greater when applied to hairy skin, suggesting a surface penetration through hair follicles or pores. Recently, studies have emerged that have actually quantified the percentage of nanomaterial that breached the stratum corneum and migrated further into the dermis or traveled to distal organ sites.^{19,41,42} However, the fate of these nanoparticles, when applied to human skin, is still not completely understood. In particular, the damage to resident fibroblasts that are numerous in the skin and most capable of immune excitation has not been thoroughly examined.

Few studies have been published which investigate the ability of CeO₂, TiO₂ or ZnO to cause DNA damage.^{43–46} As mentioned before, this data are fairly inconsistent and needs further investigation. More specifically, additional information is needed regarding the mechanism by which these particles exert DNA damage, if at all. Trouiller *et al.* reported that mice that were given Degussa P25 TiO₂ in drinking water gave rise to γ -H2AX-positive cells, but at high doses of 50–500 ppm, among which micronuclei were formed at the highest 500 ppm

concentration.⁴⁶ Another study using TiO₂ and ZnO in a dermal context found that their particles could catalyze oxidative damage to DNA (determined via the comet assay) in cultured human fibroblasts.⁴⁷ Sharma *et al.* also reported significant DNA damage from comet assay results in primary human keratinocytes with 14 ppm ZnO.⁴⁵ Auffan *et al.* found that, in human dermal fibroblasts (HDF), a concentration as low as 6 ppm could induce significant single strand breaks and binucleate cells.⁴³ Furthermore, a study of the mechanistic effects of DNA damage response (DDR) is needed on a more detailed level, while considering the nanoparticle physicochemical property influences.

A few studies have shown recently that some nanoparticles can cause cell cycle arrest in response to DNA damage. For example, G1 arrest was observed in mouse lung epithelial cells exposed to C60 and single-walled carbon nanotubes,⁴⁸ and carbon black coated with benzo(a)pyrene gave rise to S-phase arrest in human lung epithelial cells.⁴⁹ Additionally, AshaRani *et al.* reported that starch-coated silver nanoparticles induced concentration-dependent G2/M phase arrest and DNA damage in human glioblastoma cells and fibroblasts.⁵⁰ Silver nanoparticles were also found to induce S and G2/M phase arrest in Jurkat T cells,⁵¹ but no G1 arrest in RAW264.7 macrophages⁵² using similar concentrations of nanomaterials. Additionally, SiO₂ nanoparticles induced G2/M arrest in human embryonic embryo cells.⁵³ A perturbation of the cell cycle associated with an accumulation of cells in S-phase leading to cell death, is typical of compounds inhibiting DNA synthesis.^{54,55} Eukaryotic cells enter mitosis via cdc2 kinase activation, a process which includes cyclin binding and phosphorylation of cdc2 at Thr161.⁵⁶ However, activation of cdc2 during progression into mitosis requires the critical regulatory step of dephosphorylation of cdc2 at Tyr15 and Thr14.⁵⁷ Therefore, cells arrested or partially arrested in the S-phase leading up to the G2/M phase will express higher levels of p-cdc2 (Tyr15).

This work is an effort to elucidate the DDR mechanism potential in a dermal model exposed to three metal oxide nanomaterials, while considering the influence of physicochemical characteristics of the nanoparticles. Human dermal fibroblast cells were utilized to investigate these physiological effects. Fibroblasts are the most common cell-type in the dermis, and their ubiquity makes them more

appropriate for this study than the rare patrolling macrophages. Contact with the skin is one of the major routes of both intentional and accidental exposures to nanoparticles. We postulate that smaller particle agglomerates and their corresponding large zeta potentials will generate more ROS-driven DNA damage, as compared to nanoparticles which have agglomerated more severely upon contact with the cell surface.⁶⁶ In this study, changes in viability and protein expression are measured, as well as differences in ROS generation, resulting in DNA damage and cell cycle arrest. These studies examining the toxicological effects stemming from nanoparticle exposure are examined utilizing an *in vitro* system to model human health effects.

2. Materials and Methods

2.1. Nanoparticle characterization

CeO₂ (Sigma Aldrich, St. Louis, MO), TiO₂ (Evonik, Parsippany, NJ) and ZnO (Sigma Aldrich) hydrodynamic diameter and zeta potential were measured using a Zeta Sizer Nano Series ZEN 3600 Spectrometer (Malvern Instruments Ltd, Malvern, Worcestershire, UK). Particle characterization was performed on the particles suspended in Milli-Q ultrapure water (18.2 mΩ), as well as in Dulbecco's modified eagle medium (DMEM) supplemented with 10% fetal bovine serum (FBS) at 0 h, 24 h and 48 h time points. Samples were bath sonicated for 30–60 s immediately before dynamic light scattering (DLS) analyses. Manufacturer's reported primary particle size was < 25 nm, 21 nm and < 100 nm for CeO₂, TiO₂ and ZnO, respectively. The nanoparticle concentration used for the DLS and Zeta potential measurements was 50 ppm (micrograms of material per milliliter of aqueous solution). The algorithm used to transform the spectroscopy data to particle size was Stokes–Einstein; the dataset is based on intensity for size measurements. All samples were conducted in triplicate. Transmission electron microscopy (TEM) analysis was done to determine the primary particle size of the three particle-types. In general, the nanoparticle powder of each type was dispersed in 200 proof ethanol (anhydrous, ≥ 99.5% from Sigma-Aldrich) and was sonicated with probe sonicator for 30 s to 60 s right before TEM sample preparation. The TEM specimen was then prepared by dip

coating a TEM copper grid into the nanoparticle dispersion solution, followed by complete solvent evaporation in a well-ventilated hood before imaging. The specimens were examined on FEI Tecnai G² Twin High Resolution Transmission Electron Microscope at 200 kV incident beam energy. Brunauer–Emmet–Teller (BET) analysis using an accelerated surface area and porosimetry analyzer was employed to determine the surface area of the three particle-types (Micromeritics Instrument Corporation, ASAP202, Norcross, GA). Prior to analysis, samples were degassed at 110°C for 2 h.

2.2. Cell culture and experimental dosing

Cryopreserved primary HDF cells (PCS-201-010, American Type Culture Collection, Manassas, VA) were cultured in DMEM supplemented with 10% FBS (Gibco, Austria). Media were supplemented with an antibiotic cocktail consisting of penicillin, streptomycin and amphotericin (Sigma-Aldrich). Incubation took place at 37°C with humidity and 5% CO₂. Cells were grown to 80% confluency in well plates, then exposed to nanoparticles (20 ppm final exposure concentrations) or untreated for a negative control. Cells treated with nanoparticle suspensions were very briefly exposed to light in the cell culture hood at the points of exposure and harvesting. Cellular incubations with nanoparticles took place in the dark.

2.3. Cell viability

HDF cells were cultured in 24-well plates, as described above. Cells were then exposed to CeO₂, TiO₂ or ZnO to give final well concentrations of 0, 10, 50, 150, 200 or 500 ppm to generate dose-response data. Cells treated for 24 h or 48 h were rinsed three times, trypsinized and resuspended in cell culture media. Percentages of viable cells were measured by mixing equal volumes of cell suspension and trypan blue stain, followed by membrane permeability-based counting in an automated cell counter (Countess, Invitrogen). Viability experiments were done in quadruplicate. A two-tailed one sample *t*-test was employed using GraphPad Prism 6 (La Jolla, CA) software to calculate significant change in viability, as compared to the untreated control samples.

2.4. Reactive oxygen species generation

Intracellular oxidant production was measured after incubation with 20 ppm cerium oxide, titanium dioxide or zinc oxide nanoparticles every 10 min for 6 h and at 1 h, 6 h and 24 h. Briefly, cells in 96-well plates were incubated with 200 μM nonfluorescent DCFH-DA (2',7'-dichlorofluorescein-diacetate) in DMEM with 10% FBS for 30 min, then rinsed. Freshly prepared nanoparticle suspensions in new media were added to the cells. The cells were rinsed twice in phosphate buffered saline (PBS) before reading in deionized phosphate buffered saline (DPBS). Hydrogen peroxide was utilized as a positive control at a concentration of 200 μM. Relative fluorescence of the enzyme-cleaved DCFH molecule was determined in a fluorescence microplate reader (BioTek Synergy MX, Winooski, VT) utilizing an excitation/emission spectra of 480/530 nm. All responses were reported as a percentage of untreated control cells. Experiments were carried out with eight replicates per nanoparticle type. A two-tailed one sample *t*-test was employed using GraphPad Prism 6 (La Jolla, CA) to calculate significant increases in fluorescence, as compared to the untreated control samples. Additionally, separate plates of cultured and treated cells were imaged after 1 h exposures. Cells were imaged at a total magnification of 200X with an Olympus IX71 inverted fluorescence microscope (Center Valley, PA). Images were processed with Olympus CellSens software.

2.5. Protein expression alteration

HDF was cultured in the same conditions as above. Nanoparticle-treated and untreated cells were washed in ice cold 1X PBS, then protease inhibitor cocktail (Sigma-Aldrich) and high salt lysis buffer were added to the wells. Protein was isolated by collecting the supernatant via centrifugation. Samples were loaded into 6–12% SDS-PAGE gels and run at 120 mV. Gels were transferred to polyvinylidene fluoride (PVDF) membranes, which were blocked in 5% milk or bovine serum albumin/phosphate buffered saline tween (BSA/PBST) and incubated in primary antibody solutions overnight at a concentration of 1:1000: p-p38, (Cell Signaling Technology Danvers, MA), HMOX-1, (Santa Cruz Biotechnology, Santa Cruz, CA), superoxide

dismutase-1 (SOD1), (Cell Signaling Technology), p-p53, (Cell Signaling Technology), p-cdc2, (Cell Signaling Technology) or H2AX, (Cell Signaling Technology). Secondary antibody (Goat, anti-mouse or anti-rabbit, 1:5000, Santa Cruz) was prepared in fresh 5% milk or BSA/PBST solution and incubated at room temperature. Immobilon™ Western Chemiluminescent horseradish peroxidase substrate (Millipore, Billerica, MA) was added to membranes and film exposures were taken. β -actin, 1:10 000 (Sigma, St. Louis, MO) was used as a loading control. Blots shown are representative of several independent experiments.

2.6. Comet assay

Primary HDF were cultured as explained above and exposed to 20 ppm cerium oxide, titanium dioxide or zinc oxide nanoparticles for 24 h. The comet assay was then conducted under alkaline conditions. Briefly, treated cells were washed, trypsinized and suspended in agarose before being placed onto comet assay slides. Slides were then immersed in pre-chilled lysis solution for 30 min, then placed in alkaline unwinding solution consisting of 200 mM NaOH and 1 mM EDTA. Slides were then drained and electrophoresed for 40 min at 220 mA. Slides were rinsed thoroughly in water, followed by a wash in 70% ethanol. Slides were allowed to dry, then SYBR green (SG1; Molecular Probes, Eugene, OR) was directly applied to the wells. SlowFade Gold (Invitrogen, Carlsbad, CA) was also applied and allowed to cure in the dark for 24 h to stabilize fluorescence for imaging. A total of 70 images from each sample type were selected for the experiment, which was carried out in duplicate. Cells were imaged at 200X total magnification with an inverted fluorescence microscope (Olympus IX71, Center Valley, PA). DNA damage was expressed as the tail moment using an image analysis computerized method (CometScore, TriTek Corporation, Sumerduck, VA). A two-tailed one sample *t*-test employed GraphPad Prism 6 (La Jolla, CA) software to calculate significant changes in DNA damage, as compared to the untreated control samples.

2.7. Immunocytochemistry

HDF cells were cultured on sterile coverslips in 6-well plates and exposed identically to the viability experiments described in Sec. 2.3. Double strand

break inducer, etoposide, was utilized as a positive control (10 μ M) for comparison purposes. Rinsed cells were then fixed in 4% paraformaldehyde. Cell membranes were permeabilized with a 0.25% (v/v) Triton X-100/PBS solution. Cells were blocked in 1% BSA/PBST with 0.3 M glycine for 30 min, then incubated in a 1:500 primary antibody dilution (γ H2AX, CellBiolabs) with 1% BSA/PBST for 1 h. Goat anti-rabbit 647 AlexaFluor labeled secondary antibody (Invitrogen, A21244) in 1% BSA/PBST was used at a 1:4000 dilution for 1 h with all samples. Cells were rinsed several times and counterstained with 400 nM DAPI for 1 min. Coverslips were mounted onto glass slides with a drop of Pro-Long SlowFade (P36934, Invitrogen). Slides were imaged at a total magnification of 600X with an Olympus IX71 inverted fluorescence microscope (Center Valley, PA). Images were processed with Olympus CellSens software.

2.8. Cell cycle alteration

To determine the potential presence and location of cell cycle perturbation after nanoparticle exposures, HDF cultured to 80% confluency in 6-well plates were treated with 20 ppm nanoparticle suspensions for 6 h or 24 h. Both nanoparticle-treated cells and control cells treated with an equal volume of Milli-Q water were collected via trypsinization, centrifuged and suspended in PBS. Cells (1×10^6) were fixed in 70% ethanol for 2 h on ice, then held at -20°C overnight before suspension in a propidium iodide/Triton X-100 staining solution with RNase A. Flow cytometry was performed using excitation and emission spectra of 488 nm and 585 nm with a fluorescent activated cell sorter (FACS) instrument (Becton Dickinson FACSCalibur, Franklin Lakes, NJ) for DNA content evaluation. Data were analyzed utilizing DNA content frequency histogram deconvolution software (ModFit LT). Dead cells and aggregates were excluded from analysis by gating cells in a FL2-A versus FL2-W scatter plot.

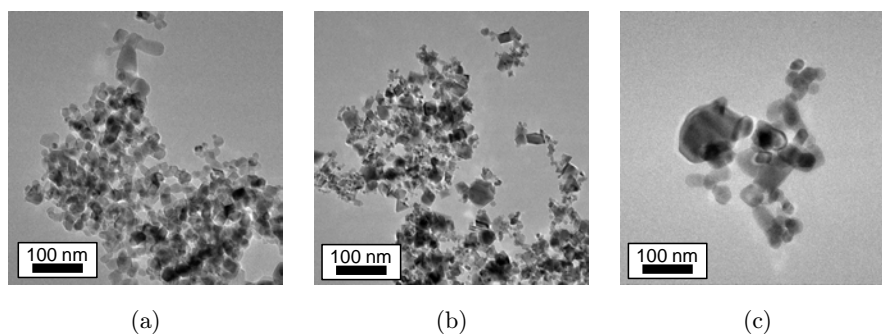
3. Results

3.1. Determination of nanoparticle size, agglomeration state, surface charge and surface area

DLS and zeta potential measurements were taken at 0 h, 24 h and 48 h in both water and cell culture

media (see Fig. 1). Changes in DLS and zeta potential readings over time reveal trends. As zeta potential migrates further from zero (neutral), agglomeration state decreases. This phenomenon could be due to a combination of competing reactions including the suspension media buffering the nanoparticle system plus the possible dissolution of zinc ions from the ZnO particles. The decrease in zeta potential for TiO₂ is not significant enough to prevent agglomeration, however. A sharp drop in ZnO zeta potential (−9.24, −11.05 and −34.00 at 0 h, 24 h and 48 h, respectively) relates with decreasing particle size (249.5 nm, 51.57 nm and 37.89 nm at 0 h, 24 h and 48 h, respectively), which is represented in Supplemental Fig. 2. The significant negative zeta potential at 48 h is deviated far

enough from zero to maintain smaller particle agglomerates. As shown in Figs. 1(a)–1(c), TEM analysis revealed polydisperse particles for all three particle-types. Qualitative observation of the TEM images indicates particle size range of ~10–50 nm for CeO₂, sub-10 nm to ~50 nm for TiO₂ and ~10 nm–100 nm for ZnO. Different particle shapes were also observed from TiO₂ and ZnO particles. BET analysis yielded surface area values of 50.441 m²/g, 59.138 m²/g and 11.625 m²/g for CeO₂, TiO₂ and ZnO, respectively. These values correspond with particle size measured by TEM analysis. Perhaps the most important finding was that CeO₂ and TiO₂ remained severely aggregated over time in complete media, whereas ZnO aggregated initially, but decreased in agglomeration state



Hydrodynamic size as measured by DLS

	0 h		24 h		48 h	
	<i>water</i>	<i>media</i>	<i>water</i>	<i>media</i>	<i>water</i>	<i>media</i>
CeO ₂	143.83 ± 5.08	324.53 ± 4.68	890.87 ± 175.75	225.27 ± 7.59	1248.5 ± 577.58	329.43 ± 9.00
TiO ₂	767.80 ± 48.25	850.63 ± 50.35	919.47 ± 267.99	321.30 ± 19.14	1118.93 ± 298.74	1130.97 ± 165.71
ZnO	1155.00 ± 163.80	249.50 ± 123.90	118.73 ± 73.19	51.57 ± 3.26	25.77 ± 6.45	37.89 ± 15.83

(d)

Surface charge as measured by zeta potential

	0 h		24 h		48 h	
	<i>water</i>	<i>media</i>	<i>water</i>	<i>media</i>	<i>water</i>	<i>media</i>
CeO ₂	8.64 ± 3.36	−10.80 ± 0.70	−9.89 ± 1.89	−10.83 ± 0.12	−7.37 ± 0.43	−11.10 ± 0.66
TiO ₂	0.03 ± 0.03	0.02 ± 0.04	−11.23 ± 0.60	−10.83 ± 0.67	−2.45 ± 8.40	−9.98 ± 0.92
ZnO	−10.18 ± 1.18	−9.24 ± 0.39	−22.97 ± 4.28	−11.05 ± 1.64	−10.23 ± 0.42	−34.00 ± 0.00

(e)

Fig. 1. Nanoparticle characterization reveals trends in toxic capability. TEM (a)–(c), DLS (d) and zeta potential measurements (e) of 20 ppm CeO₂, TiO₂ and ZnO in water and complete media at 0 h, 24 h and 48 h.

over time. By 48 h, the hydrodynamic size of ZnO decreased nearly to its primary particle size.

3.2. Concentration-dependent cell death

HDF cells treated with CeO₂, TiO₂ and ZnO exhibited dose-dependent (10–500 ppm) cell death, as determined via the trypan blue assay (see Fig. 2). A differential cell death over dose response was observed when comparing ZnO exposures to TiO₂ and CeO₂ exposures at both 24 h and 48 h. For all particle-types, cell viability decreased significantly as a function of nanoparticle dose. Brightfield images, which display the differential results after exposure to these three materials are also provided to show changes in morphology at 6 h and 24 h (see Supplemental Fig. 1).

3.3. Reactive oxygen species generation and resulting oxidative stress

To investigate the potential role of oxidative stress as a mechanism of metal oxide toxicity, intracellular oxidant production was measured after incubation with 20 ppm CeO₂, TiO₂ or ZnO nanoparticles. Separate plates of cells were treated and analyzed individually after 1-h exposure [see Fig. 3(a)]. Differences in intracellular oxidant production were observed with CeO₂ and ZnO exposure, which caused increases in ROS generation, as compared to

untreated cells. H₂O₂ (200 μM) was also utilized as a positive control. All treated samples were normalized to untreated cells. Fluorescence was also measured at 6 h and 24 h (see Supplemental Fig. 2), but fluorescence intensity was slightly higher at the 1-h time point. Representative images of cells processed identically to those read photo-spectrometrically are provided [see Fig. 3(b)].

Western blot analysis was performed to assess specific perturbation of oxidative stress proteins [see Fig. 3(c)]. HDF were exposed for 6 h and 24 h to CeO₂, TiO₂ and ZnO. Oxidative stress, as indicated by an increase in HMOX-1, is upregulated at 6 h and 24 h with exposure to ZnO. A similar trend was evident with the phosphorylation of oxidative stress and DNA damage protein, p38, where ZnO induced a distinct isoform of the protein. Induction in lysates at 24 h was similar to untreated cells, except in ZnO-treated cells. SOD1 was upregulated with CeO₂ exposure, as compared to untreated control cells. This finding was most obvious at 6 h.

3.4. Nanoparticle-induced DNA damage

A combination of single and double stand break DNA damage was measured in a comet assay [see Fig. 4(a)]. HDF cells were exposed to 20 ppm CeO₂, TiO₂ and ZnO. Damage was measured after 24 h and is reported as tail moment. An untreated control was included for comparison. ZnO caused

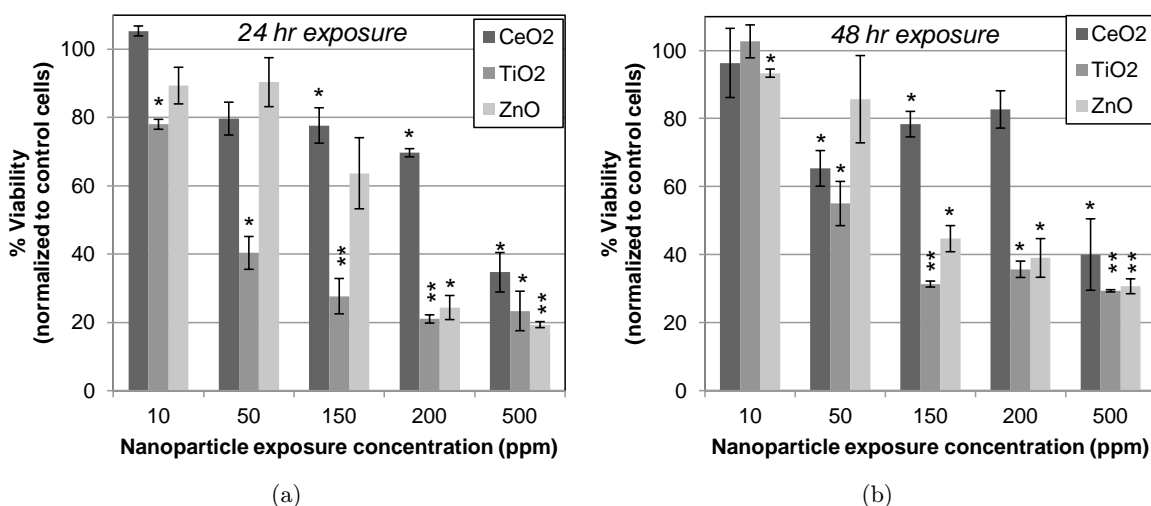


Fig. 2. Cell death correlates with increasing nanoparticle exposure. Percent viability after 10, 50, 150, 200 and 500 ppm CeO₂, TiO₂ and ZnO, as determined via a trypan-blue exclusion assay. Measurements were taken at both 24 h (a) and 48 h (b) and are normalized to untreated cells. *Statistically significant ($p < 0.05$) compared to untreated cells. **Statistically significant ($p < 0.001$) compared to untreated cells.

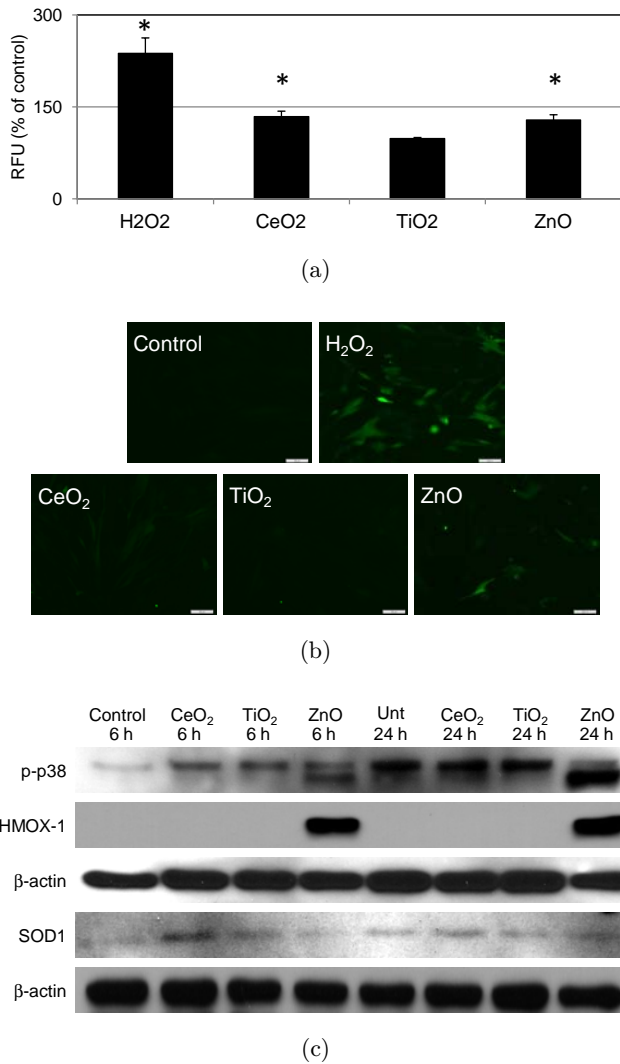


Fig. 3. Nanoparticle-driven ROS generation and oxidative stress. Intracellular oxidant production was measured after incubation with 20 ppm cerium oxide, titanium dioxide or zinc oxide nanoparticles at 1 h (a). Fluorescence images correspond to graph (b). Hydrogen peroxide was utilized as a positive control at a concentration of 200 μ M. All responses were reported as a percentage of untreated control cells. *Statistically significant ($p < 0.05$) compared to untreated cells. Upregulation of oxidative stress proteins was measured via western blot after 6 h and 24 h exposure to 20 ppm CeO₂, TiO₂ and ZnO (c). Phosphorylated p38, HMOX-1 and SOD1 protein levels were assessed in primary HDF cells following these exposures. β -actin served as a loading control. Blots are representative of three identical experiments.

the most significant amount of strand breaks. Representative images are included for comparison [see Fig. 4(b)].

Western blot analysis was performed to assess specific perturbation of DDR pathway proteins [see Fig. 4(c)]. Cdc2, a marker of cell cycle progression to

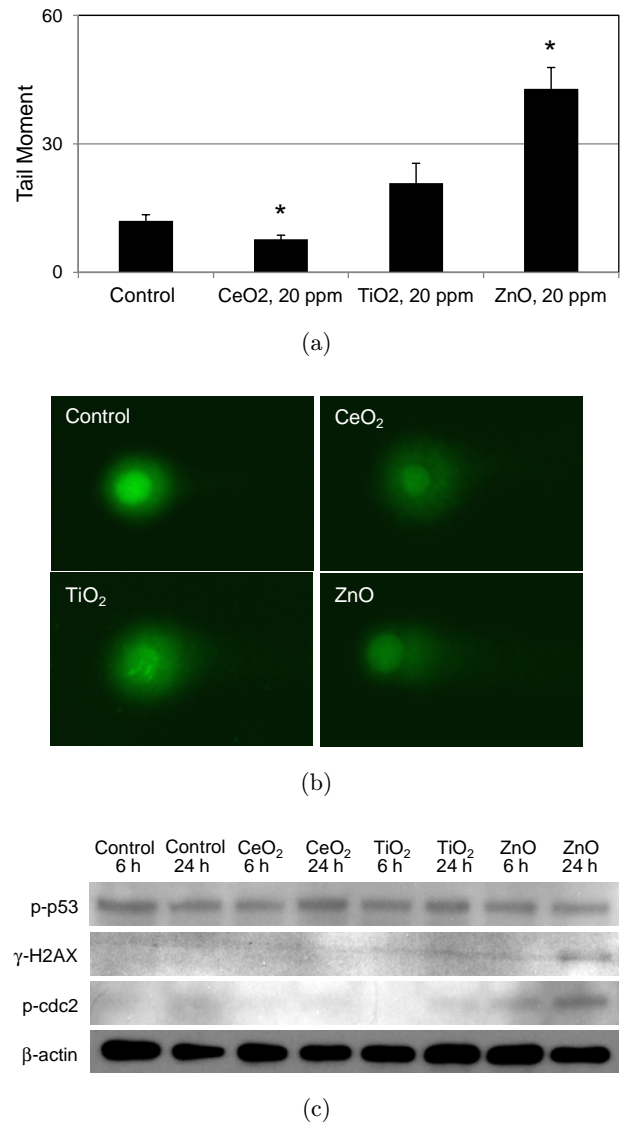


Fig. 4. Calculation of DNA strand break damage. Single and double strand break DNA damage was assayed after HDF cells were exposed to 20 ppm CeO₂, TiO₂ or ZnO (a). Cells were analyzed after 24-h exposure in a comet assay. Undosed control cells were included for normalization purposes. A total of 70 cells were imaged per treatment group. Representative images from each treatment group are included (b). *Statistically significant ($p < 0.05$) compared to untreated cells. **Statistically significant ($p < 0.001$) compared to untreated cells. Western blot analysis of DDR pathway-related protein expression after 6 h and 24 h exposure to 20 ppm CeO₂, TiO₂ and ZnO was performed (c). Activation of γ -H2AX histone variant, as well as phosphorylation levels of p53 and cdc2 were investigated and compared to untreated control cells. β -actin served as a loading control. Blots are representative of three identical experiments.

mitosis, is also phosphorylated in both ZnO-treated samples and slightly with TiO₂ treatment at the later time point. The cell cycle is allowed to progress to mitosis when cdc2 becomes dephosphorylated at

Tyr15. Therefore, an accumulation of p-cdc2 indicates halting in the S-phase. Specific double strand break repair protein γ -H2AX is only induced with 24-h ZnO treatment. A lack of expression of activated H2AX with the other nanoparticles suggests that ZnO is the only particle-type that induces DNA double-strand breaks (DSBs). This damage pathway is p53-independent, as notable changes in band intensity were absent for this protein at 6 h and 24 h. Phosphorylation of p53 was also absent at multiple time points from 0–4 h (data not shown).

Immunocytochemistry in ZnO-treated cells revealed notable DNA double strand breaks, as evidenced by a marked increase in the presence of γ -H2AX foci in HDF exposed to 20 ppm concentrations at 24 h (see Fig. 5). Moreover, foci in ZnO-treated cells were visibly more punctuate, indicating increased condensation of chromatin. Compared to untreated control cells, a slight increase in the number of foci are also present in CeO₂ and TiO₂-treated samples (see Supplemental Fig. 3).

3.5. Cell cycle perturbation

Cell cycle arrest is a critical component of the DDR, as it allows sufficient time for DNA damage repair to occur before progression into mitosis, thereby protecting genome integrity. We examined the effect of three metal oxides on the cell cycle using propidium iodide coupled with flow cytometry. At 6-h exposure, ZnO induced S-phase arrest in HDF cells, whereas no changes were observed in CeO₂ and TiO₂-treated cells, in comparison with water-treated cells [see Fig. 6(a)]. After 24-h exposure, ZnO continued to cause S-phase arrest [see Fig. 6(b)]. When compared to untreated cells at this time point, CeO₂ and TiO₂ caused less severe arrest. At the later time point, percentages of cells in G0/G1, S and G2/M phases were 78.9%, 9.3% and 11.9%, respectively for water-treated cells, 67.3%, 16.1% and 16.6% for CeO₂-treated cells, 61.8%, 18.9% and 19.3% for TiO₂-treated cells, and 46.4%, 35.8% and 17.9% for ZnO-treated cells. S-phase arrest is indicative of DNA damage and consistent with repair taking place.

Figure 7 outlines the DDR after exposure to nanoparticles. DNA strand breaks activate ataxia telangiectasia mutated (ATM) and/or attenuated total reflectance (ATR) (ATM- and RAD3-related), which initiate the DDR cascade. We have found that p38 is activated with ZnO exposure, leading to

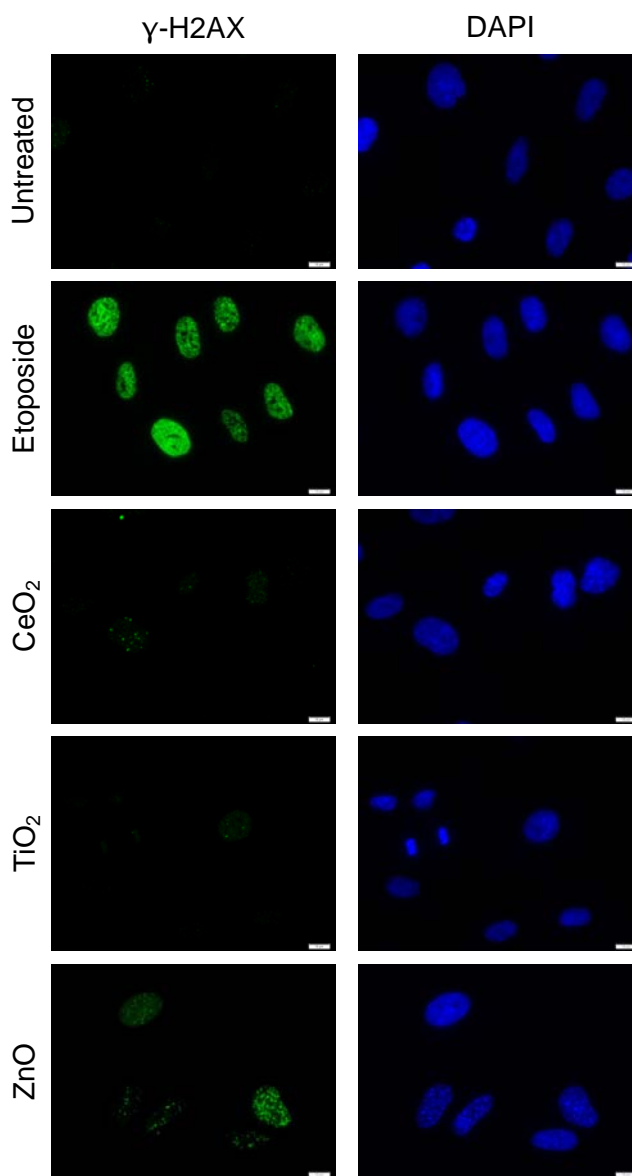


Fig. 5. DNA strand break damage, as shown by immunocytochemistry. Differential γ -H2AX expression in HDF treated with 20 ppm nanoparticles for 24 h. DAPI was used as a nuclear control. Etoposide was utilized at a concentration of 100 μ M for 1 h as a positive control. Untreated cells were also included for comparison purposes. ZnO-treated cell images indicate the most significant double strand break damage compared to untreated control cells. *Statistically significant ($p < 0.05$) compared to untreated cells. **Statistically significant ($p < 0.001$) compared to untreated cells. Scale bar = 10 μ m.

an accumulation of phosphorylated cdc (Tyr15), which further indicates cell cycle arrest. Our finding that S-phase arrest was induced by ZnO is consistent with the remainder of our results indicating significantly increased levels of ROS production, decrease in viability, protein expression and DNA

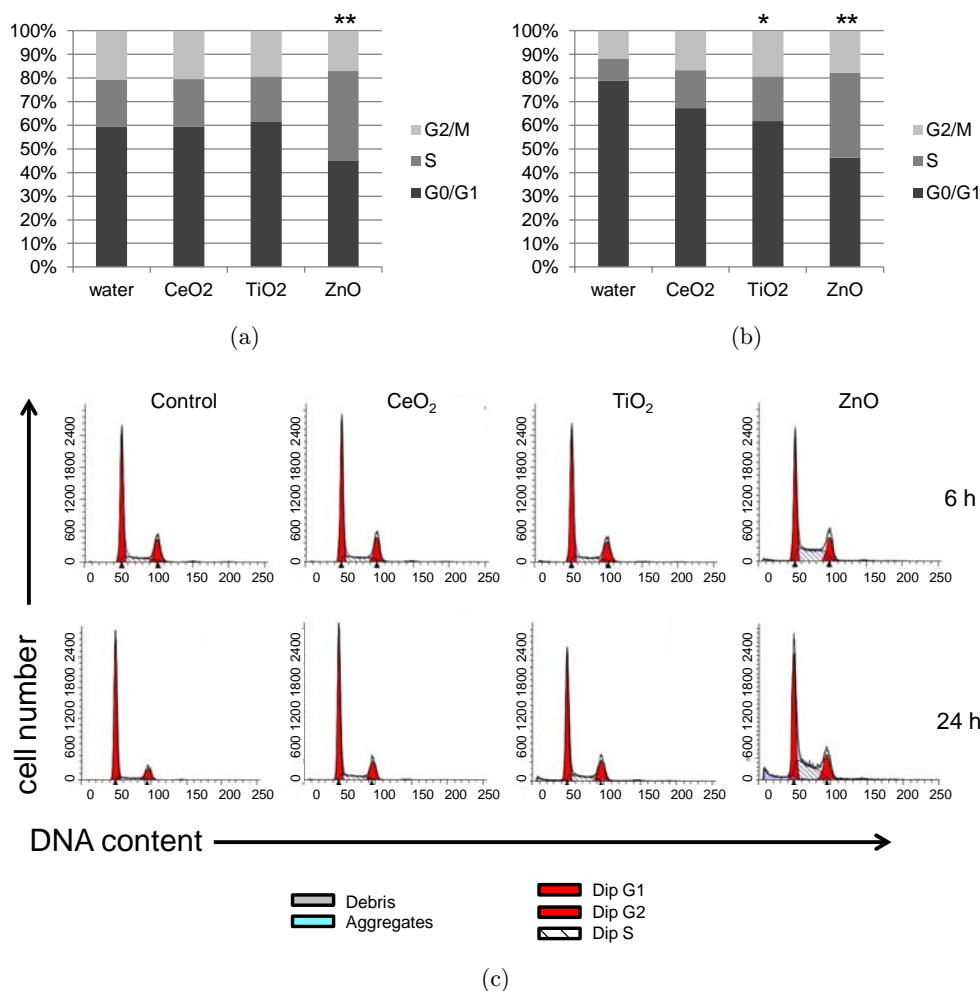


Fig. 6. Cell cycle perturbation. Changes in cell cycle were assayed via FACS after exposure to 20 ppm CeO₂, TiO₂ or ZnO for 6 h (a) and 24 h (b). Following nanoparticle treatments, cells were ethanol-fixed and stained with propidium iodide for analysis. Histograms are provided (c).

damage levels. Interestingly, none of the materials tested induced the better-studied p53 pathway, which is known to play a role in the DDR and apoptosis. P21 was also unaffected at time points from 0–4 h, 6 h or 24 h (data not shown). As previously stated, p38 has been shown to act independently of p53 in inducing cell cycle arrest. Herein, we elucidate a mechanism behind the DDR in primary HDF exposed to low concentrations of CeO₂, TiO₂ and ZnO nanoparticles.

Eom and Choi recently published results of studies in Beas-2B human bronchial epithelial cells treated with nanosized silver, where they found activation of the p38 pathway leading to S and G2/M phase cell cycle arrest with H2AX phosphorylation at 12 h and 24 h in silver.⁵¹ The same investigators also published findings in 2009 of ROS-induced p38 phosphorylation in Beas-2B cells after

CeO₂ exposures, but did not investigate DNA damage potential.⁵⁸ Here, we have assessed ROS generation and stress, as well as DNA damage potential in primary human cells resulting from exposure to three metal oxides found in commercially available products.

4. Discussion

While engineered nanoparticles possess many interesting physical and chemical characteristics, the possibility of DDR in cellular systems exposed to these novel materials needs further evaluation due to the fact that people themselves and their environment are exposed to products containing metal oxide particles on the nanoscale at an increasing rate. Differences in the responses among particle-types also need to be systematically investigated

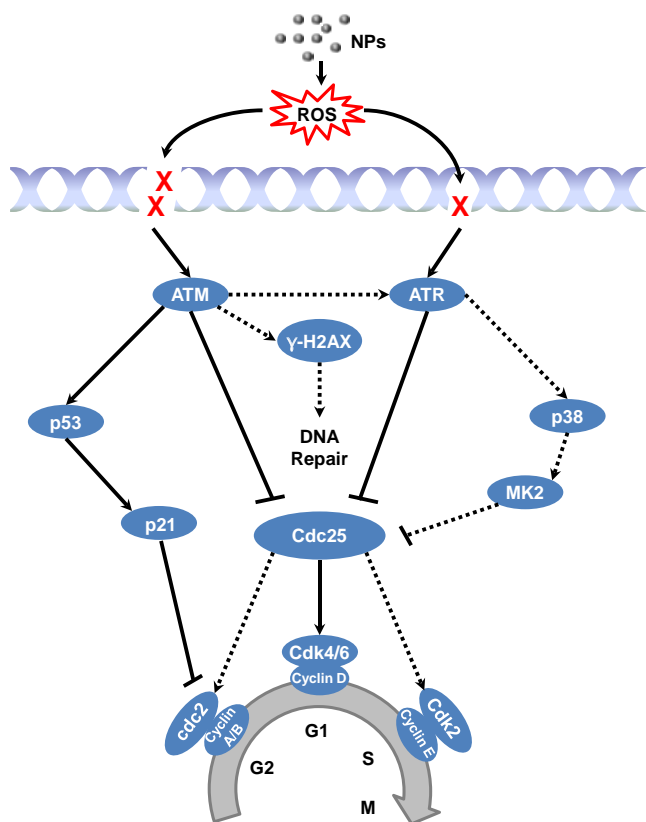


Fig. 7. Proposed schematic of HDF DDR pathway and related protein involvement after nanoparticle exposures.

since the physicochemical properties of each nanomaterial differ greatly. A mechanism by which researchers can relate biological damage with specific properties of the materials in question is, arguably, one of the most needed conclusions. Our conclusions, herein, contribute to the knowledge-base of DNA damage and repair in primary cells exposed to CeO_2 , TiO_2 and ZnO nanoparticles, while considering the role of nanospecific physicochemical properties in induced genotoxicity.

Nanoparticle characterization revealed distinct differences between particle-types. These distinct differences (such as particle size, agglomeration state, surface charge and propensity to leach metal ions) assist in explaining the observed differential toxicities. ZnO remained close to its primary particle size in culture media over time, while CeO_2 and TiO_2 became severely aggregated over time. Aggregation state of these materials was closely correlated with the zeta potential exhibited at each time point. ZnO became increasingly negative, compared to the other two particle-types, decreasing particle-particle interaction, and possibly

increasing the likelihood of interactions with cellular membranes. Additionally, Zn^{2+} ions are known to dissociate from ZnO in dermal exposure scenarios and this fact is noteworthy since zinc is an essential trace element capable of competing for cell surface receptors and initiating cell death pathways when in excess. In fact, the presence of “free” zinc ions may be the cause of ROS-driven cytotoxicity, rather than the presence of zinc-containing nanoparticles.⁵⁹

CeO_2 caused oxidative stress, as the DCFH-DA assay and SOD1 protein expression results suggest; but, significant DNA damage did not occur at this concentration. This may be due to the fact that CeO_2 did not remain in its primary particle size and likely did not dissociate into ions intracellularly, unlike ZnO .^{60,61} TiO_2 also induced some level of oxidative stress, as indicated by a slight increase in DCF fluorescence detection, but no significant DDR occurred at the concentration and the time point assessed.

5. Conclusion

Although ZnO has been found to be superior to TiO_2 as a sunscreen and cosmetic ingredient since it is more protective against long-wave UVA and is less opaque upon application,⁶² it may be more damaging to DNA in the underlying dermal tissue than TiO_2 or CeO_2 at the concentration tested. While many have found penetration of similar nanoparticles to be limited to the stratum corneum or only occasionally reaching the viable epidermis,^{30,63,64} others have found that exposures over time or factors such as flexing of the skin before application of such particles dramatically increases the depth and amount of translocation.^{19,26,41,65} It is not unreasonable to assume that metal oxide nanoparticles may be applied daily in the form of cosmetics or sunscreens, which fill the hair follicle and are then less likely to be removed during skin cleansing. It is critical that *in vivo* studies considering such realistic, confounding exposure scenarios continue, keeping in mind the potential for ROS-driven DNA damage with metal oxide exposures.

Acknowledgments

The authors would like to thank Dr. Roger Smith and Dr. Alicia Marroquin-Cardona, Texas A&M University, for assistance with the FACS

experiment, and BET analysis, respectively. Pat Chen also graciously contributed to FACS sample preparation. This work was partially funded by the Departments of Veterinary Physiology & Pharmacology and Veterinary Pathobiology at Texas A&M University. CMS also thanks the Product Quality Research Institute (PQRI) for financial support of this research.

References

1. Académie des Sciences and Académie des Technologies, Science and Technology Report No. 18 Nanosciences and nanotechnologies, Available at <http://www.tinyurl.com/nqwdda>, Environmental Health Perspectives (2004).
2. S. F. Hansen *et al.*, *Nanotoxicology* **1**, 243 (2007).
3. Nanoscale Science Engineering and Technology Subcommittee, The national nanotechnology initiative: Strategic plan, US National Science and Technology Council (2004).
4. The Royal Society and The Royal Academy of Engineering, Nanoscience and nanotechnology: Opportunities and uncertainties. Available at <http://www.nanotec.org.uk>. (2004).
5. M. Auffan *et al.*, *Nat. Nanotechnol.* **4**, 634 (2009).
6. M. J. Osmond and M. J. McCall, *Nanotoxicology* **4**, 15 (2010).
7. R. Dai, "Biotechnology in the US — Industry Risk Rating Report", IBISWorld Industry Report 54171 Scientific Research & Development in the US. Santa Monica, CA: IBISWorld Inc. (2010).
8. C. Schmidt, *Environ. Health Perspect.* **117**, A158 (2009).
9. J. Knowland *et al.*, *FEBS Lett.* **324**, 309 (1993).
10. E. Damiani *et al.*, *Free Radic. Biol. Med.* **26**, 809 (1999).
11. M. A. Mitchnick, D. Fairhurst and S. R. Pinnell, *J. Am. Acad. Dermatol.* **40**, 85 (1999).
12. N. Serpone, D. Dondi and A. Albini, *Inorganica Chim. Acta.* **360**, 794 (2007).
13. S. Yabe, and T. Sato, *J. Solid State Chem.* **171**, 7 (2003).
14. T. Masui *et al.*, *J. Mater. Chem.* **13**, 622 (2003).
15. H. Jung, D. Kittelson and M. Zachariah, *Combust. Flame* **142**, 276 (2004).
16. T. Hochino *et al.*, *J. Non-Cryst Solids* **283**, 129 (2001).
17. M. Crosera *et al.*, *Int. Arch. Occup. Environ. Health* **82**, 1043 (2009).
18. F. Larese Filon, M. Boeninger, G. Maina, G. Adami, P. Spinelli and A. Damian, *J. Occup. Environ. Med.* **48**, 692 (2006).
19. N. V. Gopee *et al.*, *Toxicol. Sci.* **111**, 37 (2009).
20. J. Kielhorn, S. Melching-Kollmuss and I. Mangelsdorf (eds.), *Controversial Topics in the Assessment of Dermal Absorption* (World Health Organization: Dermal Absorption Geneva, 2006), pp. 112–123.
21. EPA, Nanotechnology white paper. Prepared for the U.S. Environmental Protection Agency by members of the Nanotechnology Workgroup, U.S. Environmental Protection Agency: Washington, D.C. (2007).
22. L. W. Zhang and N. A. Monteiro-Riviere, *Skin Pharmacol. Physiol.* **21**, 166 (2008).
23. X. R. Xia, N. A. Monteiro-Riviere and J. E. Riviere, *Toxicol. Appl. Pharmacol.* **242**, 29 (2010).
24. M. Senzui, T. Tanure, K. Miura, Y. Ikarashi, Y. Watanabe and M. Fujii, *J. Toxicol. Sci.* **35**, 107 (2010).
25. M. Samberg, S. Oldenburg and N. Monteiro-Riviere, *Environ. Health Perspect.* **118**, 407 (2010).
26. J. G. Rouse, J. Yang, J. P. Ryman-Rasmussen, A. R. Barron and N. A. Monteiro-Riviere, *Nano Lett.* **7**, 155 (2007).
27. G. Oberdorster, E. Oberdorster and J. Oberdorster, *Environ. Health Perspect.* **113**, 823 (2005).
28. L. J. Mortensen *et al.*, *Nano Lett.* **8**, 2779 (2008).
29. A. Isakovic *et al.*, *Toxicol. Sci.* **91**, 173 (2006).
30. B. Baroli, M. Grazia Ennas, F. Loffredo, M. Isola, R. Pinna and M. A. López-Quintela, *J. Invest. Dermatol.* **127**, 1701 (2007).
31. X. Chen and H. J. Schluesener, *Toxicol. Lett.* **176**, 1 (2008).
32. B. Gulson *et al.*, *Toxicol. Sci.* **118**, 140 (2010).
33. K. Donaldson, R. Aitken, L. Tran, V. Stone, R. Duffin, G. Forrest and A. Alexander, *Toxicol. Sci.* **92**, 5 (2006).
34. A. Nel, T. Xia, L. Madler and N. Li, *Science* **311**, 622 (2006).
35. L. K. Limbach, P. Wick, P. Manser, R. N. Grass, A. Bruinink and W. J. Stark, *Environ. Sci. Technol.* **41**, 4158 (2007).
36. A. Shimada, N. Kawamura, M. Okajima, T. Kawamatawong, H. Inoue and T. Morita, *Toxicol. Pathol.* **34**, 949 (2006).
37. G. Sonavane *et al.*, *Colloids Surf. B Biointerfaces* **65**, 1 (2008).
38. A. Vogt *et al.*, *J. Invest. Dermatol.* **126**, 1316 (2006).
39. J. P. Ryman-Rasmussen, J. E. Riviere and N. A. Monteiro-Riviere, *Toxicol. Sci.* **91**, 159 (2006).
40. C. Bennat and C. C. Müller-Goymann, *Int. J. Cosmet. Sci.* **22**, 271 (2000).
41. J. Wu *et al.*, *Toxicol. Lett.* **191**, 1 (2009).
42. T. Benn, P. Westerhoff and P. Herckes, *Environ. Pollut.* **159**, 1334 (2011).
43. M. Auffan, J. Rose, T. Orsiere, M. De Meo, A. Thill, O. Zeyons, O. Proux, A. Masion, P. Chaurand, O.

- Spalla, A. Botta, M. R. Wiesner and J. Bottero, *Nanotoxicology* **3**, 161 (2009).
44. R. Y. Prasad *et al.*, The genotoxicity of titanium dioxide and cerium oxide nanoparticles in vitro, I.S. T.D. Office of Research and Development (2009).
45. V. Sharma *et al.*, *J. Nanosci. Nanotechnol.* **11**, 3782 (2011).
46. B. Trouiller *et al.*, *Cancer Res.* **69**, 8784 (2009).
47. R. Dunford *et al.*, *FEBS Lett.* **418**, 87 (1997).
48. N. R. Jacobsen, G. Pojana, P. White, P. Møller, C. A. Cohn, K. S. Korsholm, U. Vogel, A. Marcomini, S. Loft and H. Wallin, *Environ. Mol. Mutagen.* **49**, 476 (2008).
49. R. M. Mroz *et al.*, *J. Physiol. Pharmacol.* **58**, 461 (2007).
50. P. V. AshaRani *et al.*, *ACS Nano* **3**, 279 (2009).
51. H. Eom and J. Choi, *Environ. Sci. Technol.* **44**, 8337 (2010).
52. E. Park *et al.*, *Toxicol. In Vitro* **24**, 872 (2010).
53. F. Wang *et al.*, *Toxicol. In Vitro* **23**, 808 (2009).
54. K. A. Black *et al.*, *Toxicol. Appl. Pharmacol.* **97**, 463 (1989).
55. B. Binková *et al.*, *Mutat. Res.* **471**, 57 (2000).
56. S. Atherton-Fessler *et al.*, *Mol. Biol. Cell* **5**, 989 (1994).
57. C. Norbury, J. Blow and P. Nurse, *EMBO J.* **10**, 3321 (1991).
58. H. Eom and J. Choi, *Toxicol. Lett.* **187**, 77 (2009).
59. W. Song *et al.*, *Toxicol. Lett.* **199**, 389 (2010).
60. T. Xia *et al.*, *ACS Nano* **2**, 2121 (2008).
61. A. Miao *et al.*, *Environ. Toxicol. Chem.* **29**, 2814 (2010).
62. S. R. Pinnell *et al.*, *Dermatol. Surg.* **26**, 309 (2001).
63. S. E. Cross *et al.*, *Skin Pharmacol. Physiol.* **20**, 148 (2007).
64. A. V. Zvyagin and X. Zhao, *J. Biomed. Opt.* **13**, 064031/1 (2008).
65. S. S. Tinkle *et al.*, *Environ. Health Perspect.* **111**, 1202 (2003).
66. J. M. Berg *et al.*, *Toxicology In Vitro* **27**, 24 (2013).